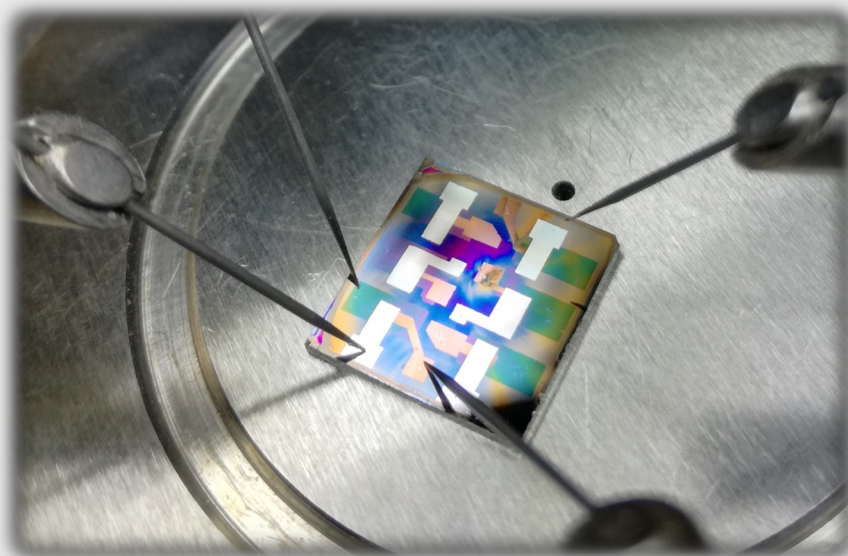End-of-degree thesis
Degree in Physics

In Device Molecular Spectroscopy in Organic Semiconductors

Author:
Elena Hernández Martínez
Co -Supervisors:
Josu Ortega Aperribay/ Luis Hueso

Leioa, the 19 of June of 2019

INDEX

Abstract

En esta tesis de fin de grado presentamos el primer estudio sobre el alineamiento energético en las interfaces entre contactos de oro y una heterounión de P3HT:PCBM. Para hacer esto, nos valdremos de un método espectroscópico denominado "in device molecular spectroscopy (i - *MOS*)". Se presentará el método de fabricación de los dispositivos con los que realizaremos la espectroscopía, transistores de electrones calientes. Seguidamente, se realizará un análisis de los resultados obtenidos con la heterounión P3HT:PCBM y los compararemos con los resultados obtenidos con PCBM, en los que observaremos el primer nivel molecular del PCBM y el un segundo nivel en el caso de P3HT:PCBM. Finalmente, se comentarán los posibles pasos futuros a seguir para continuar con la optimización de los dispositivos hechos a base de materiales orgánicos.

Gradu amaierako lan honetan urre - kontaktuen eta P3HT:PCBM heteronioaren arteko alineamendu energetikoen lehen azterketa erakusten dugu. Honetarako "in device molecular spectroscopy (i - *MOS*)" izeneko espektroskopia metodo bat erabiliko dugu. Espektroskopia egiteko erabiliko diren gailuen, elektroi beroetako transistoreen, fabrikazioa ere erakutsiko da. Ondoren P3HT:PCBM-arekin lortutako datuen analisi bat egingo da eta PCBMarekin lortutako emaitzekin konparatuko dira. Azkenik gailu hauen optimizaziorako etorkizunean egin liratekeen pausoak kontsideratuko ditugu.

In this final degree thesis a study about the energy barriers and the energy level alignments at the interface of gold contacts and a P3HT: PCBM bulk heterojunction will be presented for the first time. To do this, we will use a solid state spectroscopy method called "in-device molecular spectroscopy (i-*MOS*)". We will present the fabrication procedure of the devices used in i - *MOS,* the hot - electron transistors. After that, we will do a comparative study of the results obtained with the bulk heterojunction of P3HT:PCBM and the results using PCBM alone. We were able to observe the lowest unoccupied molecular level (LUMO) of PCBM and an extra level for P3HT:PCBM. Finally, we will consider the next steps that could be taken in order to keep optimizing the devices made with organic materials.

1. Introduction and Objectives

1.1 Organic electronics and semiconductors

In the last few decades a great interest in scientific research has raised on organic semiconductors (OSCs) and organic electronics [1,2, 4 - 8]. The motivation underlying this research is the promising characteristics that organic materials show with respect of the inorganic counterparts. It seems that these materials can be easily processed on low-cost substrates such as plastic or glass [1,2]. This fact, not only constitutes an economical advantage, but also opens a wide variety of new possibilities in the world of electronics. Furthermore, the tuneability of the functionalities and properties of organic materials makes them extremely promising. With small modifications of fundamental units, the electronic and optical properties of these materials can be modified to fulfill many emerging technological demands. In particular, organic semiconductors make posible full transparent [3], and flexible devices [4], solar cells, and solid-state lighting devices. Organic Field Effect Transistors (OFET) [5], Organic Light Emitting Diodes (OLED) [6] or Organic Photovoltaic Cells (OPV) [7] are the most common devices based on organic materials nowadays.

In order to better understand how organic electronics work, we first need to go more in deep into the theory of organic semiconductors: Organic semiconductors consist of molecules tied together by Van der Waals forces. They split in two fundamental groups, which are polymers and small molecules. Polymeric macromolecules are composed by fundamental units called monomers and therefore are soluble in organic solvents. This enables us to treat them in liquid state, which makes the deposition on chips easy, as we can spin-coat them. The small molecules materials are generally not soluble and have to be thermally evaporated [8]. The fact that Van der Waals forces couple the molecules causes a weak electronic coupling, which makes charge carrier states localized. When electrons are injected in the organic semiconductor this coupling allows them to jump from one state of an anion radical of a molecule to the lowest unoccupied molecular orbital (LUMO) of the next neutral molecule. The electronic transport mechanism works as a sequential repetition of this phenomenon. We could think of the LUMO state of the organic material analogous to the conduction band of an inorganic material. If holes are injected, this transport happens from a neutral molecule to a cation radical through the highest unoccupied molecular level (HOMO). The HOMO level can be considered as the analogous of the valence band in inorganic semiconductors. The rate in which these hopping processes happen is the conductivity of the material and is affected by many factors, such as temperature, pressure, or molecular packing and disorder. Also, the energy difference between the HOMO and LUMO levels will determine the electronic and optical properties of the material.

From an electrical transport point of view, there are three types of organic semiconductors. n - type semiconductors are those where the electrical transport is carried out mainly by electrons. If the transport is carried out mainly by holes, then the semiconductor is said to be a p-type. In the case were the transport is carried out by electrons as well as by holes we talk of ambipolar semiconductors. In this sense, organic semiconductors are very different to inorganic semiconductors, because they do not need to be doped to have this electrical transport property we just mentioned, they have it intrinsically. In fact, this property is usually determined by the energy of the molecular orbitals.

However, organic materiales present nowadays some drawbacks. For example, although organic semiconductors don not need to be doped, carriers need to be injected into the semiconductor. Even so, the transport properties of organic materiales are much lower than the ones of inorganic materials. And also, it has been pointed out that the deposition of metal electrodes on organic materials and the energy level alignment among the different constituents, has a great impact on the performance of organic based devices. Therefore, further development and research on organic materials needs to be made.

1.2 Metal/organic semiconductor interfaces

As said before, the deposition of metal electrodes can influence dramatically the electrical performance of a device composed of organic semiconductors. When a metal contact and an organic semiconductor come in touch a charge reorganization takes place at the interface and this causes the formation of an interface dipole. Thus, there is a rearrangement of the energy level alignment at the metal-organic interface and the energy difference between the metal Fermi Energy and the LUMO and HOMO molecular levels of the organic semiconductor will be increased or reduced. The energy barriers that arise at the interface limit the charge injection from the metal electrodes to the organic material. This is important at the device operative level as it determines for example the operation voltage in organic light emitting diodes (OLED) [9 - 11] or the threshold voltage of organic field effect transistors (OFET) [12,13], among others.
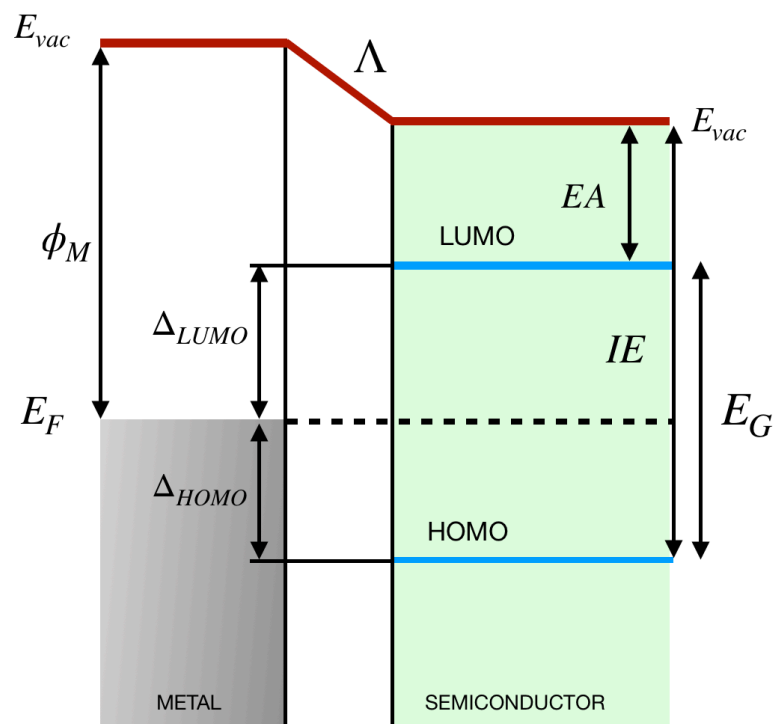

FIGURE 1.1.   **Scheme of the energy levels of a metal/organic junction.** HOMO and LUMO correspond to the highest occupied and the lowest unoccupied molecular levels. E_G is the energy gap of the organic semiconductor. E_F is the Fermi energy of the metal and ϕ_M its work function. Δ_{LUMO} and Δ_{HOMO} are the difference between the LUMO/HOMO and the Fermi

level respectively. E_{vac} represents the vacuum energy level and Λ the interface dipole. *IE* is the ionization energy of the semiconductor and EA the electron affinity.

To understand accurately the level alignment of the final device we need to consider several parameters, represented schematically in figure 1.1. E_F is the Fermi level of the metal. The vacuum level refers to the energy of a free stationary electron that is outside the material and is indicated as E_{VAC}. The difference between the vacuum level and the Fermi level is called work function and is represented by the symbol ϕ_M. The difference between the vacuum level and the HOMO is called ionization energy (*IE*), while the difference with the LUMO level is called electron affinity (*EA*). The interface energy barrier between E_F and HOMO, Δ_{HOMO} and its homologous Δ_{LUMO} are very important parameters, as these parameters together with the energy difference between HOMO and LUMO states, strongly define the electrical performance of the device. Nevertheless, their determination is not simple. It is necessary to consider some theoretical models that try to explain and represent how this alignment works. Here I present the four most common models that are conventionally used to explain the phenomena that happen at metal/organic semiconductor junctions:

1. **The Schottky-Mott model:** This model assumes that the metal and the organic interface do no interact electrically with each other, so that the interface dipole Λ is equal to 0. The energy difference of the molecular levels with the fermi level of the metal is aligned to the vacuum level at each point of the system. The electron injection barrier is the difference between the work function of the metal ϕ_M and the energy of the LUMO level of the semiconductor. The hole injection barrier is the same but with the HOMO level [14].

2. **Chemistry-induced gap states:** In the process of evaporation of metal layers on top of the semiconductor, chemical bonds between both materials can occur. This causes a creation of electronic states that may overlap with the original energy gap of the semiconductor, changing the energy scheme of the device interface [14].

3. **Induced density of interface states (IDIS):** This explains weakly interacting molecular interfaces and has to do with a penetration of the wave function of the metal in the semiconductor states. This penetration depends exponentially on the energy gap of the semiconductor. This effect increases the molecular levels at the interface and induces a density of states at the interface in the gap of the semiconductor. This phenomenon is known as induced density of energy states or IDIS [14].

4. **The "Pillow Effect":** This effect arises from the orthogonalization of the metal and organic wave functions. Considering that the electronic charge of both materials remains unchanged and using an expansion in the metal/organic wave function overlap, one obtains electron long-range interactions. This approach results finally in a reduction of the metal work function. This effect is larger for large work function noble metals like gold. However, the process followed to get to this result is too complicated and it exceed the level and ambitions of this thesis [14, 15]

A precise knowledge of the energy level and alignments is completely necessary for the understanding and profitable fabrication of devices with metal/organic interfaces, Nevertheless, the fabrication of these devices is still non-trivial. On the one hand, the production of ohmic

contacts for charge injection is complicated as the gaps between the LUMO and HOMO levels are relatively big compared to the inorganic semiconductors band gaps. On the other hand, the reactivity and brittleness of the organic materials can cause damages at the metal/organic junctions. Consequently, we had to put special care in the fabrication procedures and sequences. For example, it has been noticed that metal deposition from a hot source on a soft organic material film can induce damage into it. Also, if organic materials are evaporated or spin coated on cold metal surface abrupt interfaces can form. To avoid both inconvenient events, we had to choose opportune conditions at some stages of the fabrication process.

1.3 Measure of interface energy barriers

In this section of the thesis we will explain different methods for the measure of the interface energy barriers and alignments. We will also explain the advantages and disadvantages of each procedure and our criteria for choosing *in device molecular spectroscopy* (i-*MOS spectroscopy*).

Fundamentally, there are three procedures for the measure of interface energy barriers. First, we will explain *the direct and inverse or indirect photoemission spectroscopy* (PES, IPES). The direct photoemission spectroscopy is based on the photoelectric effect. This technique is used to determine the binding energies of electron in a substance. In the case of solid samples, the surface is radiated with ultra-violet radiation and excited electrons are emitted. The energy of the freed electrons is measured by a detector. Doing it so, it is possible to determine the energy of the HOMO level of the semiconductor. The source of the photons is usually He[1] (hv = 21.2 eV) and He[2] (hv = 40.8 eV) radiation [14]. Knowing the energy of the radiation source and measuring the number of electrons that undergo an inelastic scattering, it is also possible to provide information of the metal's work function. The formula for the work function is the one we know from the photoelectric effect:

$$\phi = h\nu - E$$

In the inverse or indirect procedure electrons are emitted towards the sample. They enter and fall into empty states [14]. Photons with the corresponding energy difference is emitted and captured by the detector. The number of photons collected due to this process contains the information about the density of unoccupied states in the material. In the case of organic molecules we obtain information about the LUMO energy level [14, 16, 17].

The problem with these characterization methods is that in order to give reliable results they require large incident electron currents, which can provoke damages in the organic layers.

Another method used is the *Kelvin probe force microscopy* (KPFM) method. With this method one determines the work function of a surface at an atomic or molecular scale due to a potential difference between the Kelvin probe conducting tip and the analyzed surface. A conducting tip scans the surface of the material at a constant high. The tip and the sample surface have usually different work functions. This creates a potential difference between both materials. A point of the sample is taken as reference, setting the potential difference between the tip and that point of the sample as zero. Then the relative potential difference at the rest

of the sample is measured. The results obtained are relative values of the work function [18 - 20]. To obtain absolute values of the work function it is possible to calibrate the tip against a reference sample with a well known work function and then start the measurement.

To study how the deposition of organic films influences the energy alignment of the material, one measures the work function before and after laying the organic film [18 - 23]. However, this study does not give us information on the possible new limitations in the carriers injection from the metal to the semiconductor. What is more, the scans done by this procedure are restricted to local regions, which makes the information obtained by this technique far from the actual working conditions of a device.

Finally, there is a last procedure for the measure of interface energy barriers, which is the *Ballistic Electron Emission Microscopy* (BEEM). The technique used along this thesis is strongly based on this method presented by J. Kaiser and L.D. Bell in 1988 [21]. The basic principle of this method relies on the use of "hot - electrons" as probes to study the energy level alignment of metal-semiconductors junctions. "Hot - electrons" are electrons that have gained high kinetic energy so that their energy is higher than the fermi level of the metal. The method employs a Scanning Tunneling Microscope (STM), to inject the hot electron via tunnelling through the barrier at the junction. Because of their high kinetic energy, these electrons overcome the energy barrier at the junction and are injected ballistically from the metal to the semiconductor material (see Figure 1.2. a) [24, 25].
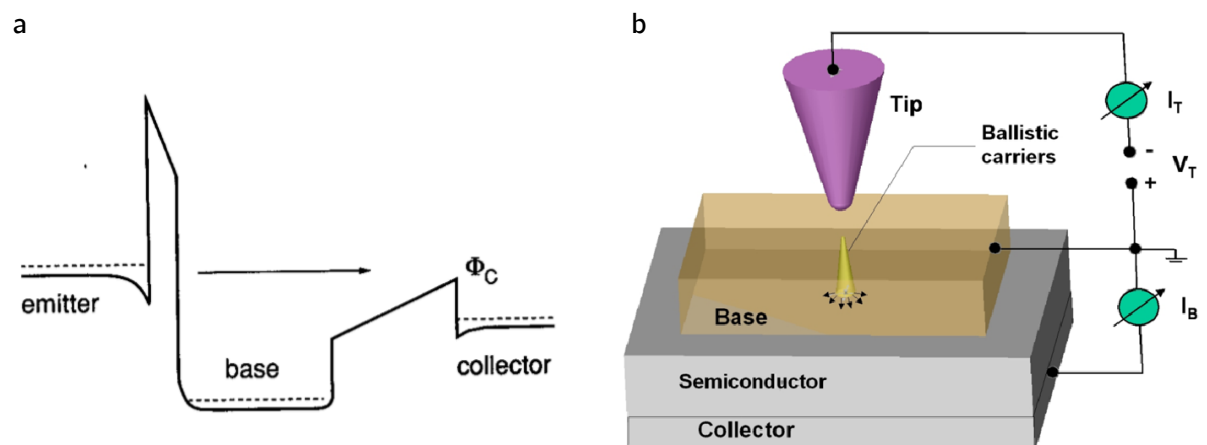

FIGURE 1.2. BEEM procedure of ballistic electron tunneling through a Schottky energy barrier. a. Due to their high kinetic energy "hot electrons" can tunnel through a potential barrier, like insulators and enter in the base zone. If the electrons have enough energy they can even cross ballisticaly the base and reach the collector [26] b. Scheme of BEEM Set - up. The tip works as the emitter, the voltage at the base is set to 0 and the current is measured at the collector. Vacuum works as an insulator. When enough voltage is applied the tip injects carriers into the semiconductor that travel to the collector and a hot electron current is measured [27].

The BEEM set up has three terminals in total. A small tip lies over the material surface. Between the material and the tip there is a vacuum region and a metal electrode, which will work as a tunnel barrier. The injection of the current is kept constant by the STM feedback loop at a certain value, while the voltage is constantly increased. While most of the injected

electrons thermalize in the base, a small fraction of them travels ballistically through the metal and encounters the energy barrier of the metal/semiconductor interface. If the voltage is high enough for the electrons to overcome the energy barrier formed at the interface, a current will be measured at the collector (see Figure 1.3.3. b) [24, 26]. Maintaining the I_E current constant assures us, that the increase in the I_C current is due to the increase in the kinetic energy of the electrons, that will therefore turn to "hot" electrons, and not to an increase of the number of electrons emitted by the tip. To achieve a constant emitter current, the distance between the tip and the surface of the substrate changes with the voltage applied. Thus, the potential barrier between emitter and base increases with the increasing voltage, which maintains the emitter current constant [21].

This characterization method has proven to be as valid as the mentioned before, as it gives the same results for known materials as the other methods. Nevertheless, it is necessary to mention that, as the methods presented above, this is also local. An improvement is required to achieve a technique that provides information of the device in working conditions. In the following section a method fulfilling this requirement will be presented.

1.4 In Device Molecular Spectroscopy

In Device Molecular Spectroscopy (i - MOS) is a solid-state spectroscopy method based on the BEEM method explained before. The fundamental difference with BEEM is that the tunnel junction made of tip/insulator/base-metal used in BEEM is replaced by a large area tunnel junction. This change allows the measurement of the metal/organic energy barrier to be non-local and therefore in device operative conditions. This is an important advantage in the applicability of the method for the development of new technologies.

As in BEEM, the set up has three terminals, the emitter "E", the base "B" and the collector "C". The emitter is an Aluminium film of approximately 13 nanometers which will be oxidized with oxygen plasma to form a thin film of aluminium-oxide insulator. This 1 to 3 nm insulator will work as the tunnel barrier. The base is composed of a 10 nanometers gold layer. The top contact is made of a 12 nanometers aluminium thin film and will collect the current that arrives from the semiconductor.

Metals tend to align their Fermi energies. This causes the Aluminium of the collector to align with the gold base. Due to this alignment there is a potential difference between the base/OSC and the OSC/Al interface. This built-in potential is convenient as it allows the charges to move from the base to the collector without any external voltage [22]. As shown in Figure 1.3. the top contact should ideally align energetically with the semiconductor, so all the current coming from the semiconductor is collected and detected. In the case of a n-type semiconductor the desired alignment should happen between the LUMO of the material and the E_F of the collector metal. For p-type semiconductor we look for an alignment between the HOMO level and E_F [22].
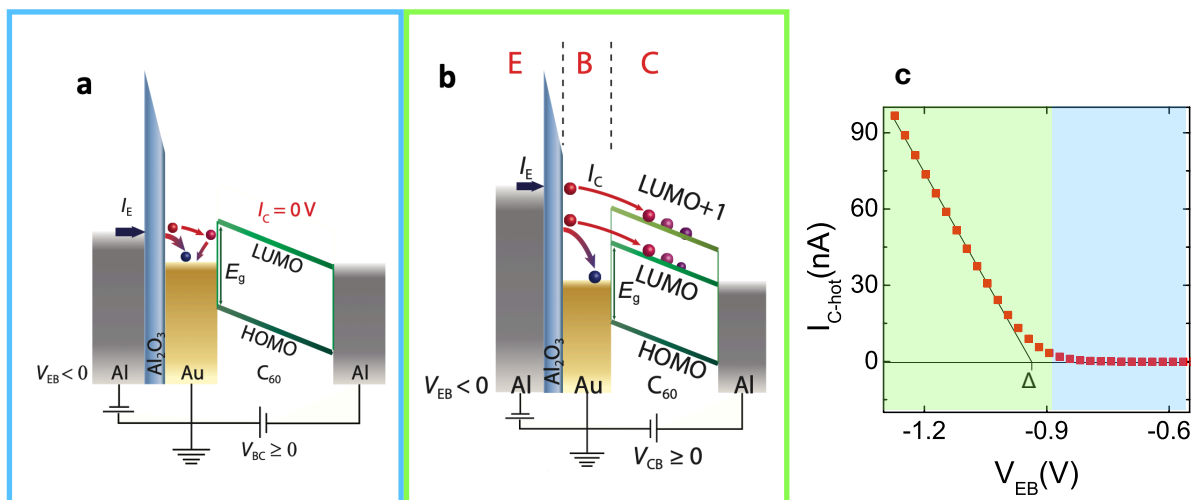
FIGURE 1.3. Working principle of the hot-electron transistor with the energy level alignment of a device made with C_{60} as OSC and expected "hot" electron current curve. **a.** The applied voltage between emitter and base is lower than the energy barrier at the metal/OSC interface, and no current can flow towards the collector. **b**. The applied voltage between emitter and base is higher than the energy barrier at the metal/OSC interface, and the current can flow towards the collector. **c**. Expected curve for a hot electron collector current in a hot - electron device. The blue part corresponds to figure a, and the green part to figure b.

The level alignment difference between emitter and base can be controlled externally with a V_{EB} ,bias. When V_{EB} < 0, electrons tunnel through the aluminium oxide barrier and as they have an energy above the E_F of the gold base they are considered "hot". Whenever the energy of the "hot electrons" is high enough to overcome the barrier, a fraction of these "hot electrons" will cross the base and penetrate the organic semiconductor without losing energy [26]. If the bias applied is high enough it would be possible for these electrons to penetrate not only the LUMO level of the OSC but also higher levels like the LUMO +1 (see Figure 1.3 b). In any case, the applied bias needs to be higher than the energy barrier between gold and OSC, as if not, the electrons will be reflected and fall to one of the states of the metal base and the collector current measured will be $I_C = 0$ (see Figure 1.3. a). If instead of a negative bias, we apply a positive one we will inject holes. The process followed by holes is analogous to the one of the electrons, but in this case the alignment between HOMO and the E_F of the collector is not convenient for the holes to be transported, so a bias between collector and base is needed. This allows us the characterization of the interface energy barriers between the Fermi energy of the metal and the HOMO and LUMO levels of the OSC.

Another advantage of using this method is that according to the Kaiser and Bell theory for inorganic semiconductors, the fitting of the I-V curves for the determination of relative molecular orbitals can be done by linear interpolation [23]. This works very well for the HOMO and LUMO levels of the OSC. For the LUMO + 1 level the determination via linear extrapolation can be frankly difficult, due to the fact that excited states have in general lower energy separations among them and that they lay usually at higher energies where the tunnelling current of the hot electron transistor is not linear anymore. Nevertheless, there are other methods to determine the relative energy of these orbitals. For example, it is possible to

look at the onset of the derivative of the *I-V* curve. However, it is easier and also effective to renormalize the collector current by the emitter current. In this way, the non linear current injection at high voltages is taken into account and the molecular levels can be clearly distinguished as an almost linear slope.

In device molecular spectroscopy enables us to determine the position of the HOMO and LUMO of the organic semiconductor for the charge transport, with respect to the Fermi energy of the base metal. By calculating the energy difference of both LUMO and HOMO levels, we can obtain the energy gap. This is the only method capable of characterizing the energy gap of OSCs and the energy level alignment of the metal/OSC interface in device operative conditions.

1.5 Objectives and structure of the thesis

In this project we aim to study the energy barriers and the energy level alignments of metal/ organic interfaces. Specially we want to analyze the behaviour of a bulk heterojunction in device operative conditions. To do this we will fabricate a hot - electron device and we will study the heterojunction with in-device molecular spectroscopy (i-*MOS*). This spectroscopy method has already proven to be successful with n-type organic materials such as C_{60} and $N2200$, as the results obtained were compatible with the ones obtained by other methods. Moreover, these studies also revealed interesting behaviours of these materials in operative conditions [23, 28, 29].

Nevertheless, the studies were carried out with n-type molecules. Our challenge is to see what happens with the energy alignments between the metals and the organic semiconductors if we introduce a p-type material in our device. Hence, we will work with an organic bulk heterojunction made with a blend of P3HT (p-type material) and PCBM (n-type material), which has never been tried before. At the same time, polymer-fullerene bulk heterojunction solar cells are a type of organic photovoltaic cells, that have shown promising characteristics with respect to their silicon based counterparts. They work with bulks made of a fullerene derivative, and a p - type material like for example P3HT [30]. PCBM is a fullerene derivative widely used in the photovoltaic industry, as it reacts strongly with light. Consequently, the study of PCBM together with a p-type material like P3HT in an i - *MOS* device can give us many interesting results for the development of optimized devices with possible new photovoltaic applications.

The following sections of the thesis are structured as follows:

Experimental method: We present the experimental techniques used to fabricate and characterize our Hot-Electron devices.

Results: We present the fabrication procedure and the results obtained with the characterization of the devices and the interpretation of those results in terms of the energy level alignments of the materials and the quality and reliability of our measurements.

Conclusions: We summarize the main results of the thesis and we comment the future projects that could be carried out in this area and the applicability of the results in the technological field.

2. Experimental Method

2.1 Fabrication equipment

2.1.1 Ultra High Vacuum (UHV) System

All the devices fabricated for this project have been produced using a system made of three interconnected ultra-high vacuum (UHV) chambers. The system consists mainly on three vacuum chambers and a load-lock. Two of the chambers are prepared for the evaporation and deposition of metals, while the last one is used for the deposition of organic molecules. The load-lock is a separate chamber, that allows the transfer of the samples without having to break the vacuum in the rest of the chambers. All the chambers have their own turbo pump systems that allow them to reach pressures of the order of 10^{-10} mbar, while the load lock stays at 10^{-7} mbar. To enter the samples into the chambers first they have to be clamped on a copper sample-holder. This sample holder will be transported from one chamber to the other through the use of magnetic manipulation arms, without having to break the vacuum of any of the deposition chambers. All of the chambers have a sample stage where the sample holder will rest with the sample during the deposition. Sample stages are cooled with a water transporting system. If necessary, they can also be cooled to 100K-150K with liquid nitrogen. In the organic chamber and the load-lock the sample stage can also be heated up via a resistance up to 250ºC. A thermocouple is used for temperature monitoring.
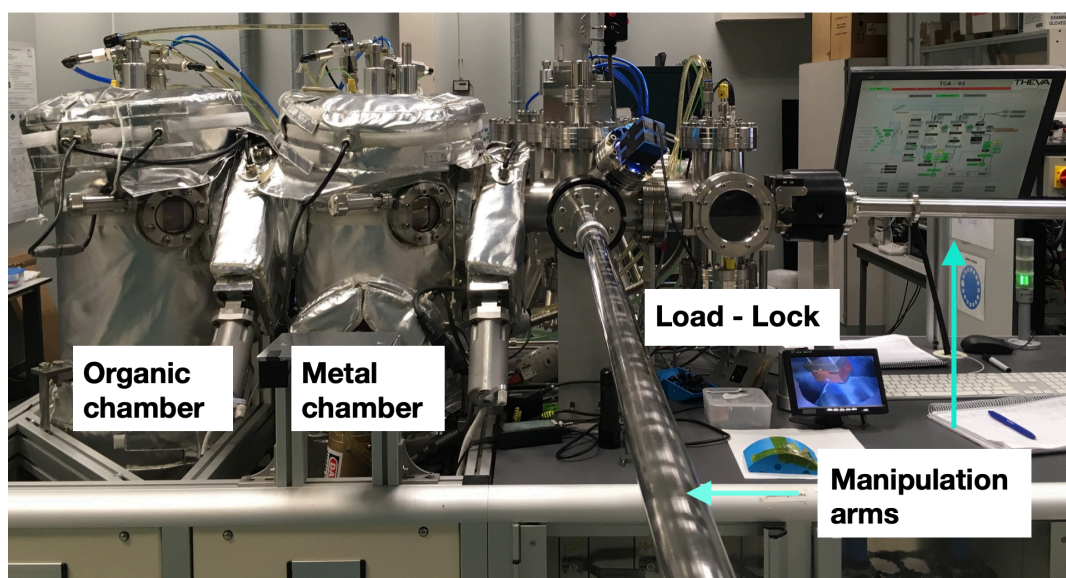

FIGURE 2.1. *THEVA*: **ultra high vacuum evaporation system.** The load - lock is used to load the samples in the ultra high vacuum system. The metal chamber is were metals are e-beam evaporated. In the organic chamber organic materials are thermally evaporated. The magnetic manipulation arms allow the user to transport the sample from one chamber to the other.

In every deposition chamber there is a crystal monitor that measures the amount of material that is being evaporated. The crystal monitor needs to be calibrated periodically for each material so that the measurements are correct. To do that, we deposit material on a sample and with X-Ray reflectivity we measure the actual thickness of the layer. Comparing this measurement with the estimation of the crystal monitor we can adjust its calibration.

The deposition chambers also contain a shutter and a shadow mask system. The shutter is placed between the sample and the material source. It makes sure the material reaches the sample when the desired evaporation rate is reached. The shutter can be opened and closed by a pneumatic actuator using a software. For the pattering of the devices we used a shadow mask system (see figure 2.2.). The masks are made out of patterned stainless steel foil. They are placed so that it covers the sample during the deposition. The system is designed in order to be aligned in each stage of the chambers. This way it is possible to stack on top of each film, other different thin films with different shapes to form the desired device. Due to this, the material is deposited in the substrate with the pattern of the shadow mask without any need of lithography techniques that would certainly damage the organic materials.
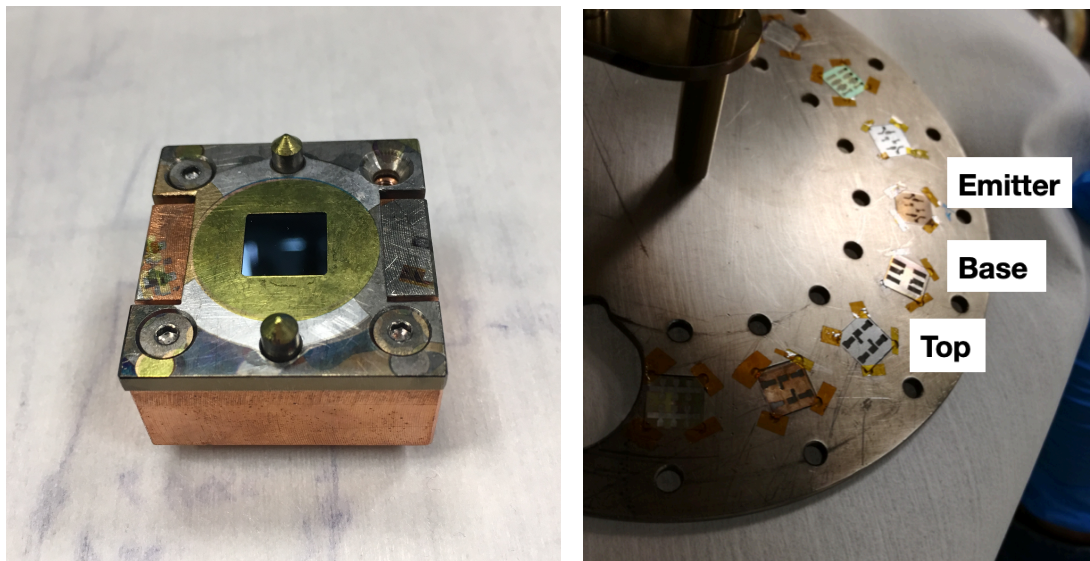

FIGURE 2.2. **Components of the UHV system. a,** The sample holder is the tool used to transport the sample inside the UHV system during the hole deposition process. **b,** The shadow mask contains the shapes for the emitter, the base and the top contact.

On the following paragraphs I will describe briefly the working principle of the chambers used for the fabrication of the hot - electron device.

i) Load - Lock

This chamber is mainly devoted to the insertion and extraction of the samples, preserving the pressure levels in the rest of the chambers. However, it has also other

useful and necessary functionalities, like the possibility of doing plasma treatments. This is fundamental for our devices, mainly for the construction of the Tunnel-Junction, which will be described later.

Low plasma treatments are done as follows: First we put the turbo pump in stand by with a reduced speed of 200Hz instead of 1000Hz, reaching a pressure of 10^{-6} mba. When this pressure is reached we can insert Argon or Oxygen (in our case will be always Oxygen) into the chamber. The gas pressure reaches 0.1 mbar, once this is so we ignite the plasma by applying a high voltage between the sample stage and a glow discharge plate. We will use this procedure to oxidize some aluminium films of the emitter, forming tunnel barriers between emitter and base. The formation of the insulating layer is strongly dependent on the timing and the power of the plasma generated in the chamber. This process can be tuned and optimized to obtain with the right recipe the desired insulating layer.

ii) *THEVA*: Metal Chamber

This chamber is used for evaporation of metals through electron-beam evaporation. A current is passed through a filament to induce thermo-ionic emission of electrons. These electrons are focused using magnetic fields, so that they form a beam directed towards the material inside the crucible. The crucible that contains the metal we want to evaporate is heated due to the impact of the electrons against it. This causes the metal to sublimate and so a portion of the evaporated material will deposit on top of the substrate. The crystal monitor records the rate at which the material sublimates and the thickness of the layer that is being deposited.
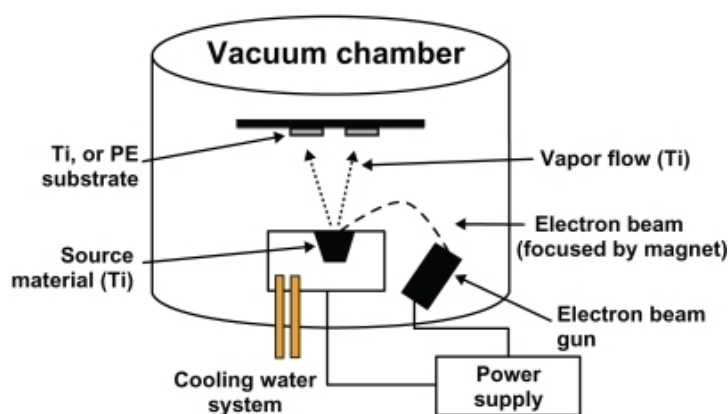

FIGURE 2.3. **Scheme of the working principle of a e-beam evaporator.** The electron beam is directed towards the material inside the crucible. While the crucible is maintained water cooled, the material inside sublimates and deposits on top of the substrate. The crystal monitor measures the deposition rate and the thickness o the deposited layer[1].

In particular *THEVA* metal evaporator has a UHV compatible *Telemark* 528 e-beam source with four crucibles. Our e-beam power supply has a 3 kW maximum power, and

---

[1] http://www.fotoimage.org/e-beam-evaporation-2/

each of the crucibles has a capacity of 1.5 cc. The distance between the material and the substrate are 20 cm, which on the one side is advantageous as this prevents the deposition of material on the chamber walls and increases the reliability of the measurements of the crystal monitor. On the other side, such a small distance between material and substrate can be a problem if we want to deposit a metal on top of an organic layer, as the radiation emitted might damage the organic material.

iii) *MANTIS*: Metal Chamber

This chamber was incorporated later to *THEVA* evaporator and although it offers the possibility of evaporating many different types of materials its use has been limited to aluminium thermal evaporation.

There are two different types of thermal evaporation. The first one is thermal boat source evaporation. The principle of this method is to put the material in a conductive boat, which will be heated by passing a high electrical current through it. As the temperature of the boat rises, the material in the boat starts to melt and then it begins to evaporate. The more current is applied, the higher is the evaporation rate of the material. The maximum possible current is 100 A, equivalent to a temperature of around 2250ºC (depending on the type of the boat and the material in it).

The second method of thermal evaporation is through effusion cells. The effusion cells are placed in a vertical position with respect to the sample and are provided with a shutter that can be manually or electrically actuated. The cells contain a wound tungsten filament to heat a Pyrolytic Boron Nitride (PBN) cylindrical crucible. The temperature is measured in several locations of the crucible and an average of the measurements is provided. The error in the temperature of the crucible is of the order of 2ºC. This allows a very accurate control of the deposition rate and the deposited layer thickness. The maximum temperature of this cells is 1300ºC.
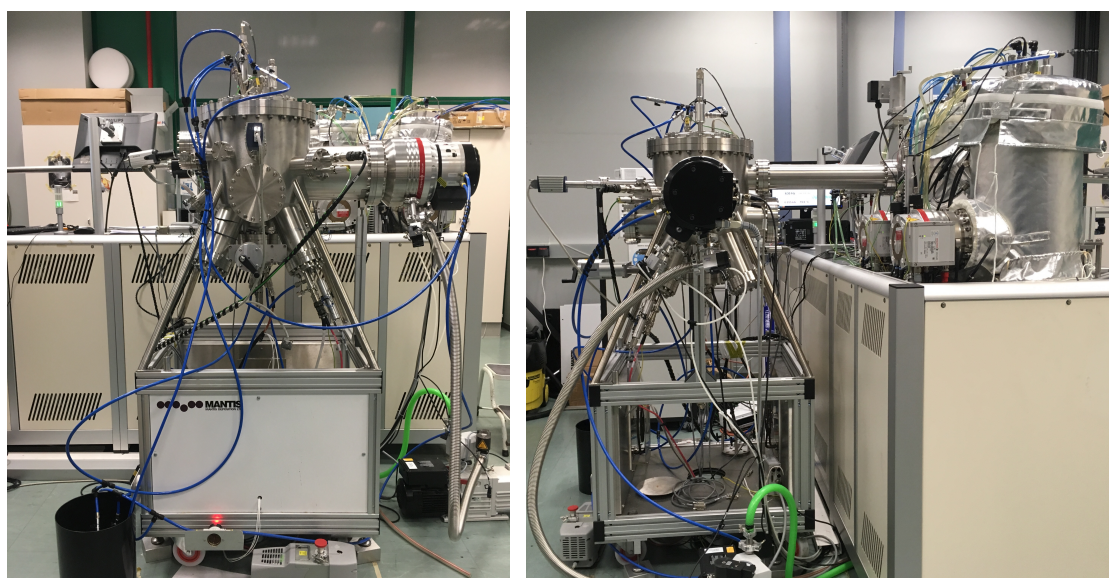

FIGURE 2.4. Metal evaporation chamber *MANTIS*. Mantis metal ultra high vacuum evaporator incorporated to *THEVA*.

iv) *THEVA*: Organic Chamber

This chamber is used for evaporation of organic materials via effusion cells. The working principle is the same as for the metal effusion cells, with the difference that in this case the crucibles are made of quartz and the operational temperature is lower. Theva organic evaporator is composed by three effusion cells (max 800ºC) and a low-temperature effusion cell (max 250ºC) from *MBE komponenten.* The organic material used are molecules in powder and the crucible that contains them is an elongated Quartz crucible from *MBE komponenten.* A little shutter over the effusion cells is maintained closed till the deposition temperature is reached. The shutter at the cells plays the role of protecting the cells from cross contamination and the chamber walls from the deposition of plenty of undesired organic material. The whole process is controlled by a software. Once the sublimation temperature is settled, the shutters open and the deposition will begin. When the desired thickness is reached the deposition ends automatically, the shutters close and the crucible is cooled.

2.1.2 Spin Coater

The Spin coater is the machine used for the spin coating. Spin coating is a procedure to deposit thin layers of material on a flat substrate. There are two types of spin coating, the static and the dynamic. In the static case a small amount of coating material is applied on the centre of the substrate, and then the substrate is set to spin. There are two parameters that will define the thickness of the layer, the acceleration and the final velocity of the spinning substrate. In the dynamic case the substrate is already spinning at a certain velocity before the coating is applied. The thickness of the layer will depend on the recipe we use for the acceleration and/or velocity of the spin coater and on the viscosity and concentration of the solution.
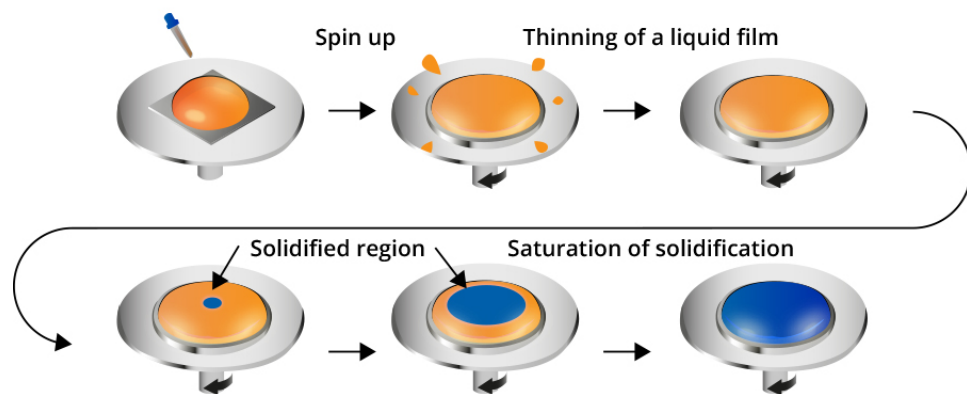

FIGURE 2.5. Spin coater work stages. First the solution is deposited. Then the fluid spins off the edges of the substrate. After that, the solvent evaporates and the thin film that stays on top of the substrate starts to solidify till it reaches a total solidification. Finally, we have a thin solid layer on top of the substrate.

2.3 Characterization techniques

In this section we will explain the methods used for the mechanical and electrical characterization of the devices.

2.3.1 Thin Film

We have used two main methods for the mechanical characterization of the samples: X-ray reflectivity and profilometry.

i) X - Ray

The X-Ray reflectivity method is based on two optical principles, Snell's law and Bragg's law.

The Snell law determines that in the interface of two materials with different refractive indexes there is a critical incident angle below which the electromagnetic wave will be completely reflected back without penetrating in the material. Above this angle, the intensity of the reflected wave decreases, till no reflection is detected. In between these two extreme cases there is a range of angles in which part of the wave will be transmitted through the organic material, while part of the wave will be reflected at the air/OSC interface. The transmitted wave will encounter another interface that corresponds to the OSC/substrate interface. Here part of the wave will be reflected again.
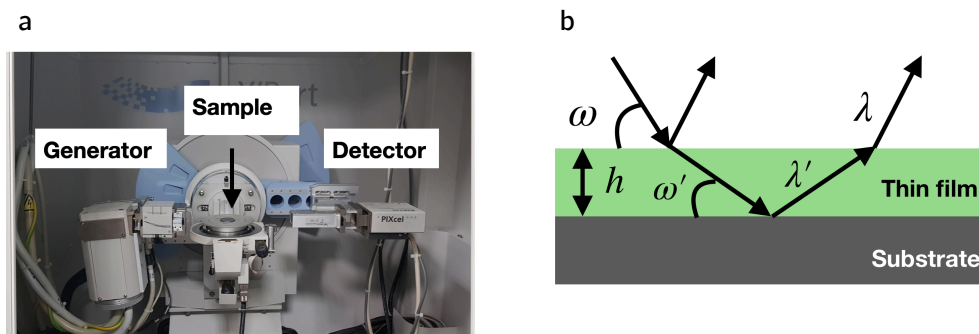

FIGURE 2.6. X-ray equipment and its working principle. a, the generator emits X-ray radiation towards the sample and the detector collects the information of the refracted incoming radiation. b, the radiation approaches the thin film surface. Part of the radiation is refracted back and part of it continues to the substrate surface where it is refracted again

These two reflected rays will interfere with each other. Depending on the optical path of each of them, they will interfere constructively or destructively forming interference peaks. The machine uses an X-ray beam with incident angles of 2 - 3 degrees and measures the rejected ray intensity, thus it is possible to scan the sample with few degrees of the incident angle.

The peak position carries information about the separation between the reflecting planes, this is the air/OSC and the OSC/substrate interfaces, which determines the thickness of the organic layer. To extract the information about the thickness we use a modified Bragg's law formula:

$$m\,\lambda' = m\left(\frac{\lambda}{n}\right) = 2d\sin(\omega_{l})$$

where λ and λ' are the wavelength in air and in the thin film, n and d are the refractive index and the thickness of the film, ω_{l} the incident angle and m the interference order.

X-ray not only gives us information about the thickness of the layer, it can also show us qualitatively the roughness of the film we are working with. In the critical case where the roughness is very high, the thin film is expected to scatter incoherently the incident ray, so that there is no interference at all. On the other hand, when the surface of the film is very flat the presence of peaks is very clear.

In short, X-ray gives us good information about the thickness of the film and some information about its roughness.

ii) Profilometer

The profilometer is a device used to measure the thickness of thin films. In our case we have used contact profilometers. This device has a diamond stylus, which is moved vertically till it is in contact with the sample. Then, it moves laterally for a specific distance and contact force and collects the information about the height differences between the structures that are encountered during the scan.
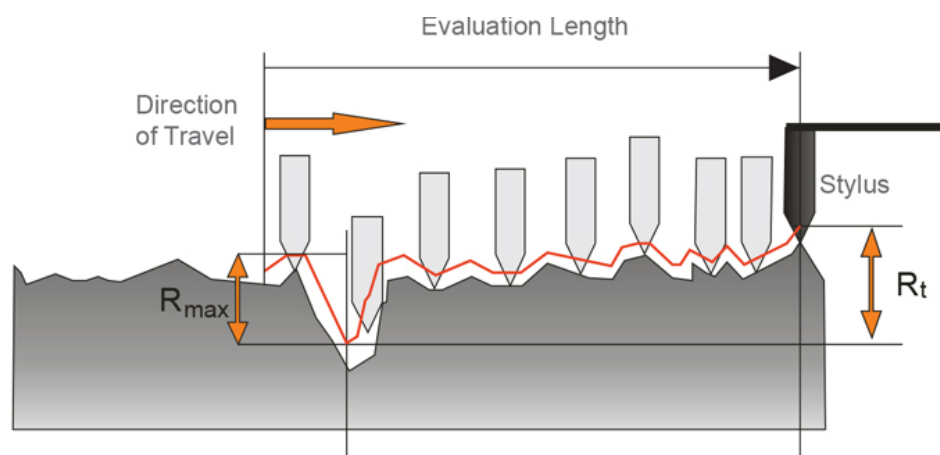

FIGURE 2.7. **Working principle of the profilometer.** The stylus travels across a previously established path and measures the height at every point along that path. The lowest point relative to the stablished zero is R_{max}. The difference between the lowest and the highest point of the surface is R_{t}[2].

---

[2] https://www.picswe.com/pics/surface-roughness-7a.html.

To know the absolute height of the different points of the measured surface one can scratch a little line till one reaches the substrate. From the line recorded during the scan is possible to set the substrate as reference and obtain the height difference at the walls of the scratch. The profilometer can measure from one millimetre to approximately 10 nanometres, and the resolution of the measurement is controlled by the speed of the stylus.

2.3.2 Electrical characterization

For the electrical characterization of the devices we carried out vertical measurements in a *Lake Shore* probe station (PS) (see Figure 2.8. a). The probe station is provided with four tips to reach the contact pads of the samples (see Figure 2.8. b) and two radiation shields that minimize the external noise. The measurements are performed in a vacuum of the order of 10^{-5} mbar. Via a compressor the sample can be cooled down to 4,9 K. When lowering the temperature the tips are thermally contracted and have to be repositioned once the system has reached a stable temperature.
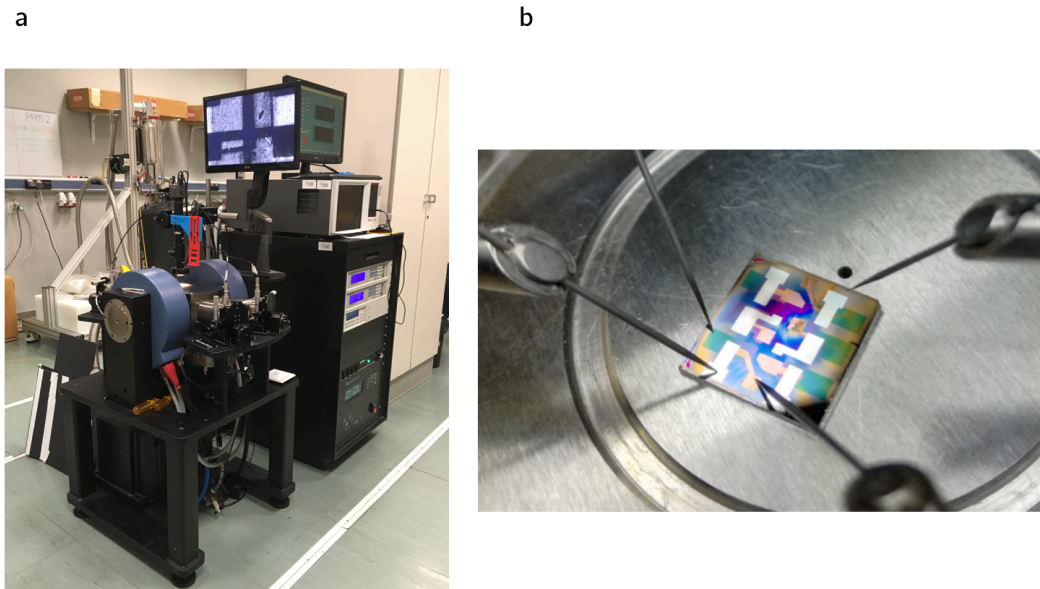
a   b

FIGURE 2.8. Picture of the probe station. a, *Semiconductor Characterization System Keithley 4200* set up. b, contact tips of the probe station over a hot-electron devices sample.

To process and control the electrical measurements we used the *Semiconductor Characterization System Keithley 4200,* equipped with three source measurement units (SMU). The triax cables used together with the radiation shield enable a nominal noise level below 10 fA. During actual measurements the tips have to touch the sample and some factors, like mechanical instability of the tips-sample contact, due to the kind of material or the thickness and roughness of the layer, can add noise to the measurement. For example, when lowering the temperature, the compressor introduces an unavoidable vibration that generates noise.

It is also possible to   apply magnetic fields up to 0.5 Tesla, however, we will not perform measurements with magnetic fields in this thesis.

The programs used to control the measurements were programmed with Labview. In particular, we have used a program to control the current-voltage (*I-V*) measurements in two terminals and another one to perform the the *I-V* three terminal measurements.

3. Results

In this part of the thesis we will present and discuss the results obtained with the hot-electron devices made with PCBM (an n - type material) and the P3HT:PCBM p - n bulk heterojunction. Both the materials are solution processable and are of great interest for photovoltaic applications.

PCBM is a fullerene (see figure 3.1), and therefore its molecular structure is similar to the already studied C_{60}. This will enable us to compare our results with the published ones for C_{60}. Moreover, we wanted to study how a p - type material like P3HT, used to form a bulk heterojunction together with PCBM, is influencing the energy level alignment with respect to the reference device made only with PCBM.
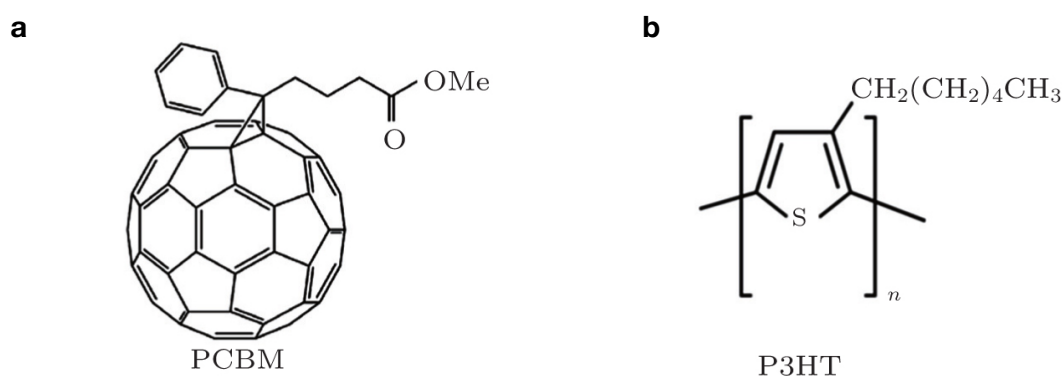
a

b

FIGURE 3.1. Scheme of the PCBM monomere and the P3HT molecule. a. Scheme of the buckyball structure of PCBM. It has a similar structure to the C_{60} fullerene. The tail ending in O and OMe makes PCBM soluble. **b.** Scheme of the structure of P3HT.

Within the same device we have examined separately the tunnel junction, the diode, which will also work as a photovoltaic cell, and the hot-electron transistor. In this way we will show how the electron are injected, the role of the bulk heterojunction in the conversion of light and to perform a spectroscopy of the energy level alignment at the metal/organic interface.

3.1 Fabrication

As explained in the introduction chapter, hot electron transistors are three terminal devices consisting of an emitter, a base and a collector. The emitter is a 13 nm aluminium contact, thermally evaporated in *MANTIS* in ultra high vacuum conditions (10^{-9} mbar) (see Figure 2.2. b) at a rate of 1 Å/s with the opportune shadow mask (see Figure 2.2. b). After the deposition of the aluminium, this is oxidized to create an Al_2O_3 layer. To oxidate the aluminium correctly we need to stabilize the plasma first. After that, the plasma oxidation is done at a pressure of 0.1 mbar and following an already well stablished recipe that consist of two minutes of plasma at 1200 V (10mA) and other three minutes at 1200 V (50mA) [31]. The two-step oxidation process helps to form a robust oxide layer. The initial lower plasma starts a uniform and slow oxidation, while the second step finishes the actual oxide layer. This

assures a barrier with a good compromise between resistance and strength at high voltages (up to 2.5 V).

The base is a 10 nm thick gold layer, evaporated in the *THEVA metal chamber* at 1 Å/s and with a pressure of 10^{-8} mbar. Gold is a noble metal, thus its properties make it a common material for device contacts in research. It also has a different work function compared with aluminium. This will cause a built-in potential between the Au/OSC interface and the Al/OSC interface. Due to this potential difference the injected electrons that arrive to the semiconductor will be pushed towards the collector without the need of any external bias.
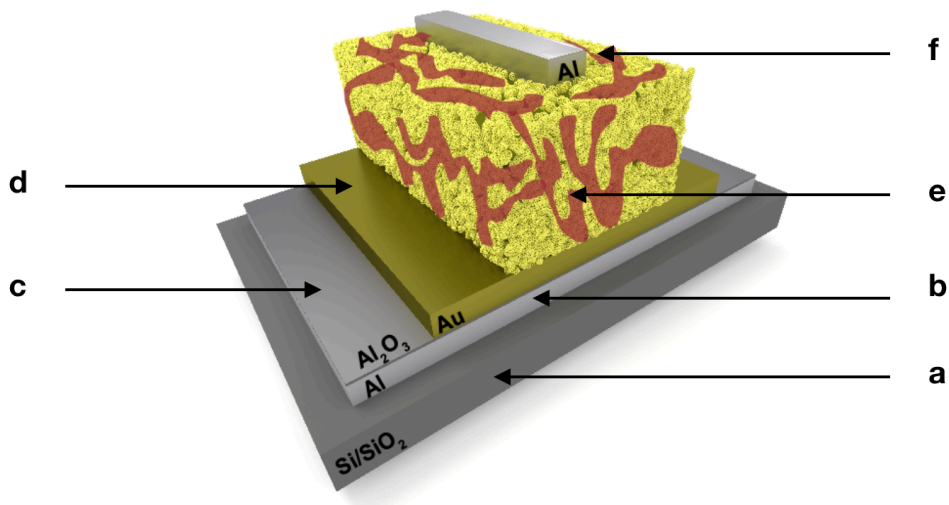

FIGURE 3.2 Scheme of the complete hot-electron transistor. a, Si/SiO_2 substrate. **b,** 13 nm thick aluminium emitter. **c,** Plasma oxidized aluminium as insulator. **d,** A 10 nm thick gold layer works as the base of the device. **e,** Spin coated P3HT-PCBM organic semiconductor. **f,** The top contact is a12 nm thick evaporated aluminium layer.

Once the emitter has been evaporated, we take the sample out of the ultra high vacuum system and deposit by spin coating solution of P3HT-PCBM (poly[3-hexylthiophene-2,5-diyl] — phenyl-C61-butyric acid methyl ester). We do this in cleanroom to improve the quality and cleanness of the OSC film.

PCBM is a soluble n-type material and is often used in organic solar cells and flexible electronics together with p-type materials like for example P3HT. The use of P3HT seemed particularly advantageous as it is soluble, it has a molecular self-assembly structure and is a widely used polymer in organic electronics. Because of these properties the use of the blend made of P3HT and PCBM seems promising for future technological applications [32]. Before spin coating the solution on the device, we first had to try this procedure on top of test substrates. The objective was to obtain a film that was as thick and uniform as possible in order to prevent short circuits between base and collector due to the interpenetration of the top contact into the OSC. The solvents selected for the tests were chloroform and dichlorobenzene.

Two main problems arose in the sample trials. The first one was the appearance under the microscope of non dissolved particles in the spin-coated layer. The second challenge was to determine the parameters to obtain an adequate thickness of the layer. The solution with chloroform was giving us more uniform films, so chloroform seemed to dissolve the P3HT:PCBM molecules better than dichlorobenzene. At the same time, increasing the concentration of the solutions to obtain thicker films, made the spin-coating procedure more challenging, because the higher volatility of chloroform, resulted in a too fast drying solution, that did not give the spin coater enough time to accelerate and to spread the solution around the sample.

For this reason we tried with the dynamic spin coating. This technique consists in the deposition of the solution while the spin coater spins at a constant velocity. This method gave as a result a uniform organic layer. We tried different velocities and spin duration for the spin coater and measured the thickness of the deposited layer in each trial with a profilometer.

The recipe that seemed optimal consisted of a stirred solution in chloroform of P3HT:PCBM (1:1) with a concentration of 20mg/mL, while for the PCBM alone we used 10mg/mL with the same solvent. Regarding the spin coating the speed was set at 3000 rpm for 60 s. The final thickness of the organic layer used in our hot - electron devices was of 80-90 nm. To be sure that no trace of the solvent remained in our diode layer we kept the sample inside the load-lock at a 10^{-6} mbar vacuum for more than two hours.

To finish the device we evaporated on top of the stack a thin film of aluminium. The choice of aluminium should   be optimal for the collection of electrons because its work function is close to the LUMO of PCBM. To avoid penetration of the top contact metal into the organic material, the evaporation is done in two steps. This procedure also helps to avoid any damages due to the hitting of aluminium particles on the organic surface while evaporating. First, we evaporate a 4 nm thick aluminium layer at a low rate of 0.1 /s. This layer is supposed to fill any roughness present in the organic surface without causing damages. After having a thin and homogenous aluminium film on top of the organic material, extra 8 nm of Aluminium are evaporated at a rate of 1 Å/s. As the evaporation rate increases, the time necessary for the evaporation decreases, so that the possible thermal damage due to prolonged evaporation is reduced.

3.2 Electrical characterization

3.2.1. Tunnel Junction

The tunnel junction is an essential part of the hot-electron device. As said in the fabrication process we have an Al/AlOx/Au structure, where the aluminium has been oxidized creating a potential barrier between emitter and base. This fabrication method has proven to be more effective than laying an aluminium oxide layer on top of the non oxidized aluminium [23]. If the plasma oxidation is done correctly the final thickness of the insulator is of 1 to 3 nm. This is fundamental for the correct functioning of the whole device. The tunnel probability decreases exponentially with the tunnel barrier thickness, so if the barrier is too big, almost no "hot" electrons will

tunnel, and no current will be measured. On the contrary, if the surface of the emitter aluminium has not been completely oxidized there will be leakage, so that not only "hot" electrons will be injected, but also thermal electrons. This event could alter our results and drive us to erroneous conclusions. For these reasons it is fundamental to verify that our tunnel junction is injecting enough "hot" electrons but that there is no leakage. It is also important to have a strong tunnel junction, that can bear high voltages, as "hot - electrons" need to have high energies to tunnel through the energy barrier.

To study the tunnel junctions of our devices we have performed two terminal measurements. When a bias V_{EB} is applied, charges are accelerated from base to emitter ($V_{EB} > 0$) or from emitter to base ($V_{EB} < 0$). The energy of the injected carriers will depend on the applied voltage. Only if enough energy is applied, will be possible for the charges to tunnel through the junction.

Figure 3.3.a shows the obtained I - V curve for the tunnel junction. The shape of the curve is the characteristic shape for our tunnel junctions. For low voltages the current increases linearly with respect to the applied voltage. For higher voltages the curve starts to deviate from the linear dependence. The $|I_E|$ current is higher for positive biases than it is for negative ones, which means that at the same voltaje the holes injection is higher than the electron injection. This makes sense, as the Fermi Level of gold is lower than the Fermi Level of aluminium (see figure 1.3).
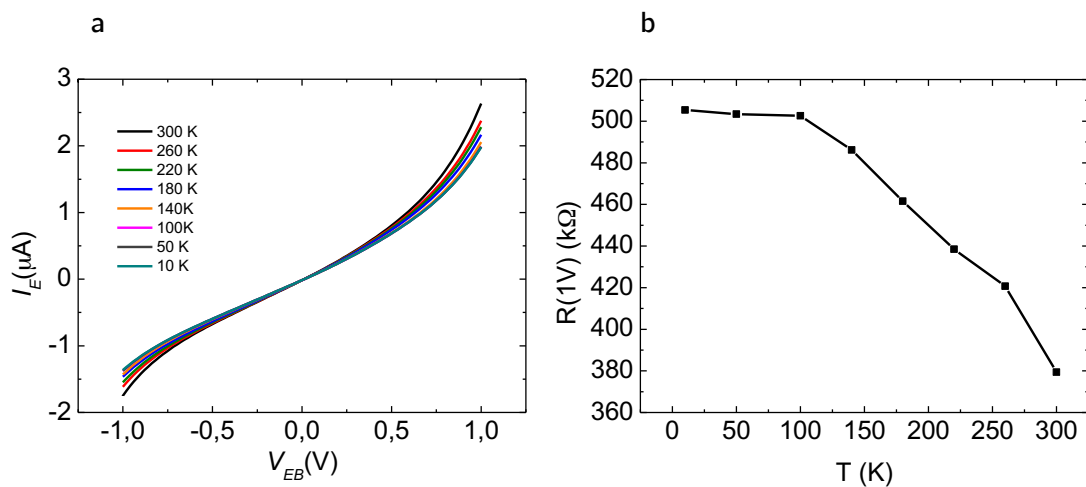

FIGURE 3.3. **Tunnel junction current and resistance. a**, Typical I - V curve of the tunnel junction. The curve increases lineally for low biases and deviates from linear behaviour at high voltages. **b**, The resistance decreases with temperature, contrary to the behaviour of metals, which is a sign of the absence of thermal electrons.

Figure 3.3.b exhibits the behaviour of the resistance of the tunnel junction with respect to the temperature of the sample. Metals are expected to have lower resistance for lower temperatures. This is clearly not the case, which means that the potential barrier is homogeneous and thick enough to not suffer from leakage. The current decreases with temperature due to the fact that "hot - electrons" have also a component of the energy related to the temperature of the sample. If the thermal energy is lower, their

total energy also decreases, which causes an increase of the resistance of the tunnel junction.

In short, the recipe used provides high reproducible and strong tunnel junctions with almost identical *I* - *V* curves, and resistance response with temperature.

3.2.2. Diode

After having discussed the tunnel junction, we move now to the electronic transport of our organic based devices. We have analyzed the transport in devices with PCBM and with a bulk heterojunction of P3HT:PCBM. For a complete study we have performed the two terminal measurements of the diodes with and without light.

First we have studied the behaviour of both diodes at room temperature without light. As shown in figure 3.4. both diodes rectify for positive values of the collector base voltage V_{CB}. This is due to the different energy alignment of aluminum and gold with the semiconductors.
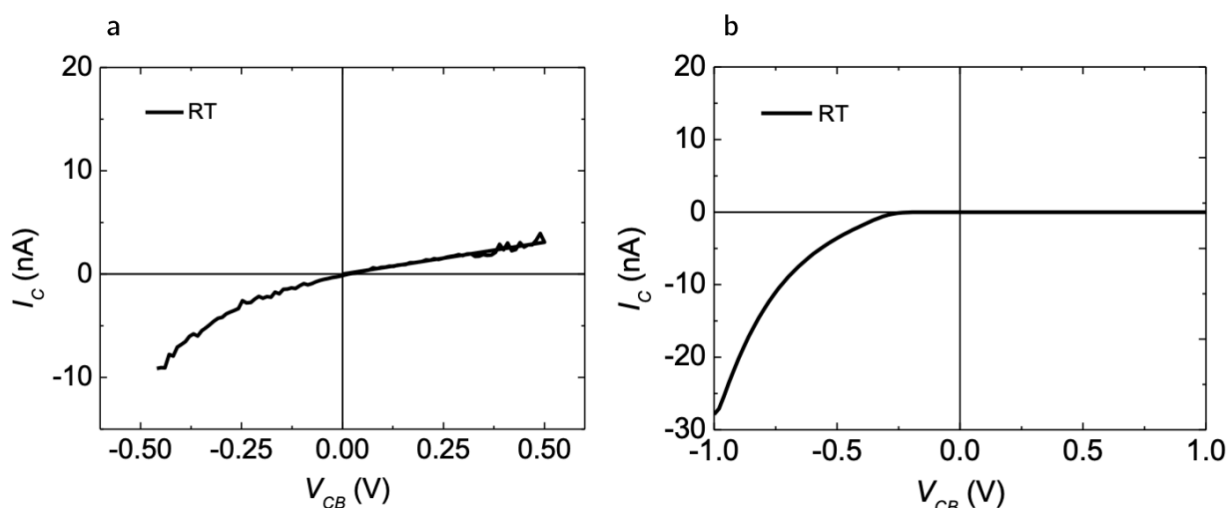

FIGURE 3.4. **Electrical characterization of PCBM (a) and P3HT/PCBM (b) without light.** *I* - *V* curves at room temperature without shining light to the device. The device works like a diode rectifying for positive biases.

For negative voltages we see a current that increases (in absolute values) with the absolute value of the voltage. This is due to the fact that aluminium aligns very well with the LUMO of PCBM (present in both of the devices), allowing electrons to pass easily to the semiconductor without the need of much energy. For positive voltages is gold the one that is supposed to inject electrons in the semiconductor. However, as there is a large energy difference between the Fermi level of gold and the LUMO level of the semiconductor, almost no electrons reach enough energy to be injected in the OSC and the current value of the collector approaches zero (see figure 3.5.). This means, that the diode rectifies for positives values of the collector - base bias. As explained in

previous chapters of the thesis, this fact is actually advantageous for us, as we need such an energy difference between Au/OSC and Al/OSC interfaces, so that injected "hot" electrons flow from the base/OSC interface to the collector without any external bias. This happens for PCBM as for P3HT:PCBM. No outstanding difference is observed between both organic layers in dark conditions.
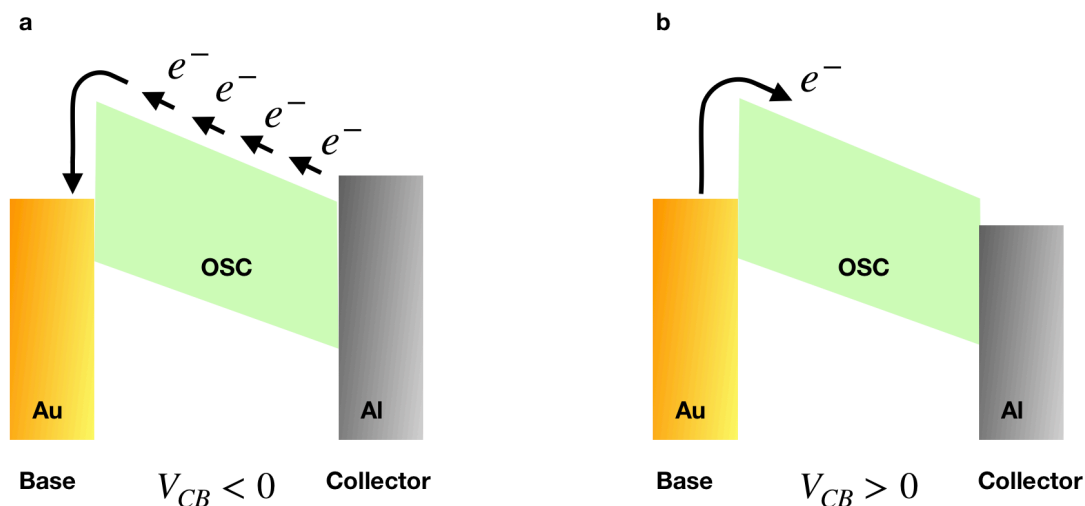

a

e^- e^- e^- e^-

OSC

Au

Base $V_{CB} < 0$ **Collector**

b

e^-

OSC

Au

Base $V_{CB} > 0$ **Collector**

FIGURE 3.5. Scheme of conduction of electrons from metal to OSC. a, Aluminium aligns well with the organic semiconductor, therefore, when a negative collector bias is applied, electrons flow easily from the aluminium to the semiconductor and towards the gold base. **b**, There is an energy barrier between gold and the semiconductor. The electrons need a big amount of energy to surpass energy barrier.

To prove the presence of P3HT and its role in the samples we analyzed the photoresponse of PCBM and of the bulk heterojunction of P3HT:PCBM to light. To do this, we exposed the sample to a source of light with a power of $7.5\dfrac{mWatt}{cm^2}$ during the measurement. The *I - V* curves obtained are shown in figure 3.7. Even if both of the devices are reacting to the light exposure, as expected, the junction with both p-type and n-type semiconductors is showing a higher response. To understand better the working principles of a photovoltaic cell, in figure 3.6 is shown an ideal *I-V* characteristic. Our results appear inverted with respect to the ideal case simply because, to maintain the base grounded, the biases are reversed with respect to the ideal situation.
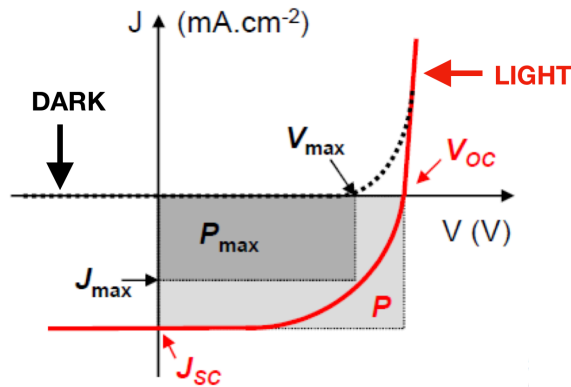
FIGURE 3.6. Ideal *I-V* characteristic of a photovoltaic cell. V_{OC} is the open circuit voltage, which corresponds to the voltage for a 0 current density. J_{SC} is the short circuit current, which corresponds to the current density at 0 collector base voltage. V_{MAX} and J_{MAX} are the values of the voltage and the current, which give the maximum power extraction of the cell.
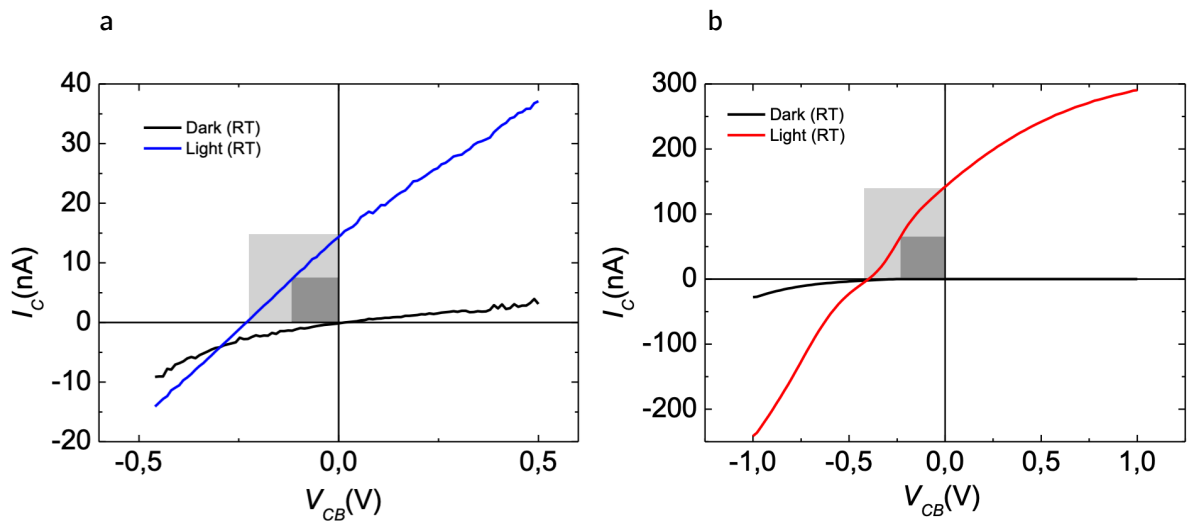

FIGURE 3.7. Electrical characterization of PCBM (a) and P3HT/PCBM (b) with light. *I - V* curves at room temperature with shining light to the device. The dark grey rectangle corresponds to the real power extraction of the photovoltaic cell, while the light grey is the ideal maximum power that could be extracted with the respective values of short circuit current (J_{SC}) and open circuit voltage (V_{OC}).

Usually, a photovoltaic cell is just a diode that, besides having rectifying properties, is also able to convert light in electricity. This is due to the fact that light induces the creation of electron - hole pairs, which are free to move inside the semiconductor (see figure 3.8). This new free electrons and holes are the source of the non zero current that is appearing in the I-V curves when light is applied even in reverse bias conditions. The power that can be extracted from such a device is calculated using the product of

the voltage and current that are maximizing the area described by the curve (dark grey area in figure 3.6).

We can compare the power that can be extracted from the photovoltaic cell in each case. Table 1 shows the extracted values that can be used for the calculation of the efficiencies of the cells.

$$\eta(\%) = \frac{FF \times V_{OC} \times J_{SC}}{P_{irr}}$$

	V_{OC}	J_{SC}	V_{MAX}	J_{MAX}
PCBM	0.24 V	14 nA	0.12 V	7.3 nA
P3HT/ PCBM	0.4 V	143 nA	0.19 V	84 nA

TABLE 1. Formula for the efficiency of the photovoltaic cell and data of the *I - V* curves for PCBM and P3HT/PCBM exposed to light. P_{irr} is the power of the irradiated light, V_{OC} the open circuit voltage, J_{SC} the short circuit current and FF the fill factor. V_{MAX} and J_{MAX} are the values of the voltage and the current, which give the maximum power of the diode.

Using the equation for the efficiency and the values obtained from the data, we can obtain what follows:

$$PCBM: \qquad V_{MAX} \times J_{MAX} = 0.876 \, \text{nWatt}$$

$$P3HT/PCBM: \qquad V_{MAX} \times J_{MAX} = 15.96 \, \text{nWatt}$$

These are the experimental values of the maximum extractable power of our photovoltaic cells. We can see already how the bulk heterojunction is producing more power than the PCBM alone.

We have also compared the efficiency of the PCBM and the P3HT:PCBM diodes. The equation used to calculate the efficiency of the diodes is the following one:

$$\eta(\%) = \frac{FF \times V_{OC} \times J_{SC}}{P_{irr}}$$

Where P_{irr} is the power of the light, V_{OC} the open circuit voltage, J_{SC} the short circuit current and FF the fill factor, which is given by:

$$FF = \frac{(V_{MAX} \times J_{MAX})}{(V_{OC} \times V_{SC})}$$

The results obtained for the efficiency of PCBM and P3HT:PCBM are the following:

$$\eta_{PCBM} = 0.00001\,\%$$
$$\eta_{P3HT/PCBM} = 0.0002\,\%$$

The efficiencies are really low so our photovoltaic cells are not directly implementable in nowadays technology. This is not a problem as that was not the goal of our experiment. As we mentioned before, the main purpose was to have an indication of the difference between the two devices. As expected the efficiency of the P3HT:PCBM bulk heterojunction is much higher (around 200% higher) than the efficiency of the PCBM diode alone. P-n heterojunctions work in general better that photovoltaic materials alone. In fact, p-n junctions are widely used in silicon based organic cells nowadays. When the semiconductor is constituted only by an n-type material like PCBM, the light excites the electrons in the material, forming free electron-hole pairs, but as the semiconductor is n-type, the energy disposal of the material causes only electrons to be transported and so a net current of electrons is formed. In an p-n bulk heterojunction we have both, an n-type and a p-type material mixed together. When the light excites the charges, both electrons and holes are transported through the n-type and p-type material, so that the net current for a certain applied light source is higher than in a n-type material alone (see figure 3.8.). This is basically the proof that P3HT is definitely part of the device under study and that we can go on with the analysis of the influence brought by the polymer on the energy level alignment.
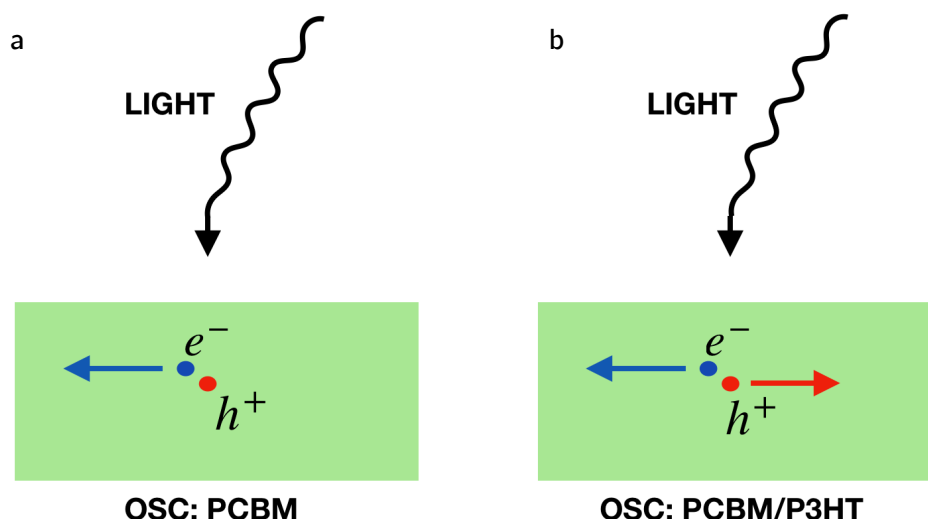

FIGURE 3.8. Working principle of the organic photovoltaic cell. **a,** An electron-hole pair is formed due to the incident light. As PCBM is a n-type material, only an electron current is established. **b**, An electron - hole pair is formed in the PCBM/P3HT heterojunction. Due to the fact that PCBM is n - type and P3HT p-type, an electron

and a hole current are formed, flowing in opposite directions. This will cause an increase in the efficiency of the cell compared to the PCBM cell.

The observable S - shape in the I - V curve with light in figure 3.7.b is a phenomenon reported in many, almost all, P3HT:PCBM solar cells, that has to do with a poor contact between PCBM and the collector. This hampers electron extraction and leads to an inequality in the rates at which holes and electrons are extracted from the semiconductor. This issue has been studied and its existence does not influence our results [34].

3.2.3. Hot - Electron device

After making sure that the tunnel junction and the diode work properly, we performed three terminal measurements of the full hot-electron transistor. The current - voltage characteristic of our hot - electron devices are shown in figure 3.9.

Accordingly to what has been explained in section 1.4 of this thesis, when a negative V_{EB} bias is applied a current I_E is injected from the emitter to the base. This current is made of "hot" electrons, because, as shown in figure 1.3, these electrons are above the Fermi level of the gold base. The current measured at the collector for negative values of the base - collector bias V_{EB} , is due to the electrons that have enough energy to overcome the energy barrier at the Au/OSC interface. These electrons cross the thin gold base ballistically without any noticeable energy attenuation.
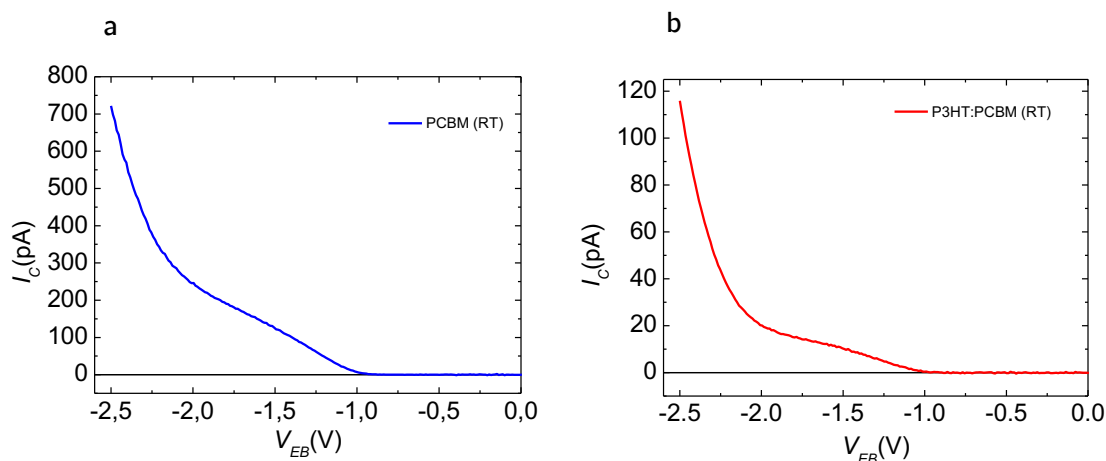

FIGURE 3.9. *I - V* curve for PCBM and P3HT/PCBM based i - *MOS* devices. **a**, "Hot" electron current of an i - *MOS* device made with PCBM (a) and P3HT:PCBM (b) for $V_{EB} \leq 0$ at room temperature. The energetic electrons are injected ballistically in the semiconductor using no collector - base voltage ($V_{CB} = 0$).

For values of V_{EB} close to zero the "hot" electrons have an energy below the energy barrier at the Au/OSC interface, so they do not manage to enter at the LUMO level of

the semiconductor and they thermalize in the base. For more negative voltages, the electrons acquire higher energies, till a small fraction of them can enter into the LUMO level of the OSC or even into other higher molecular levels [22]. For these kinds of measurements, the V_{CB} is always maintained at zero. The value of the necessary bias for this to happen will determine the energy barrier at the Au/OSC interface. From the measurements shown in figure 3.9, we can see the onset of the "hot" current. With a linear fit we can estimate that the Au/OSC energy barrier is around 1.0 eV for both PCBM and P3HT:PCBM.

It seems convenient to recall here a feature of our devices that distinguishes them from the BEEM spectroscopy. In BEEM the emitter current is maintained constant independently of the bias, due to variations in the distance between emitter and semiconductor. This is not the case in i - *MOS*. As seen in section 3.2.1 the emitter current increases with the bias applied, and this rise is not linear for high voltages. This means that, when in figure 3.9. we see that the current is increasing, this does not necessarily mean that the increase is due only to the higher energy of the electrons. It can mean that the number of excited electrons has risen and consequently the amount of hot electrons is also higher, increasing the collection of charges. This is of special importance when we look to the second change in slope of the curves, because although it could be related to the presence of an extra molecular level, it could also be related to the nonlinearity of the injected current. To avoid this effect to carry us to erroneous conclusions, we have renormalized the collector current, dividing each value by the value of the emitter current I_E. The resulting curves are shown in figure 3.10.
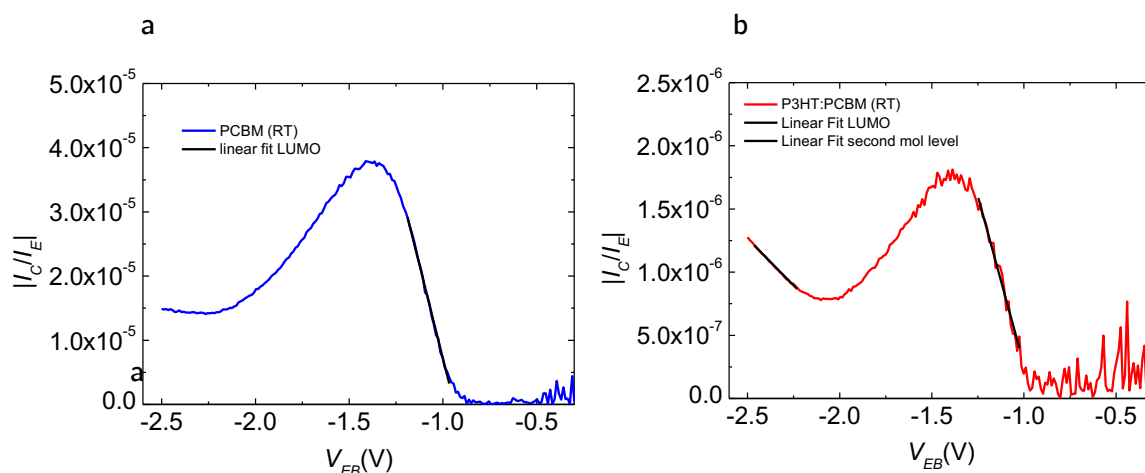

FIGURE 3.10. Renormalized "hot" electron current versus emitter - base bias. **a**, *I - V* normalized curve for an i - *MOS* device based on PCBM. The injection of "hot" electrons in the semiconductor is studied using a linear fitting. In this case we see an electron injection corresponding to the LUMO level of the PCBM **b**, *I - V* normalized curve for an i - *MOS* device based on P3HT:PCBM. The injection of carriers is linear fitted again. The curve shows two injection of electrons, one corresponding to the LUMO level of PCBM and the second one to a non - determined higher molecular level.

Figure 3.10.a shows a one large rise of the number of "hot - electrons" that approach the collector. We performed linear fits to extract the values related to the relative

energy barriers between Au and OSC. This evinces the access to the LUMO level of PCBM by "hot - electrons" starting at -1.0 eV. In the case of the bulk heterojunction of P3HT/PCBM we observe two different changes in the slope of the "hot - electron" current. The first interpreted as the filling of the LUMO level of PCBM, also at -1.0 eV. We say is the LUMO level of PCBM due to the fact that the LUMO level of PCBM has a lower energy than the LUMO level of P3HT, so we expect it to be filled first. The second one is due to the injection of electrons in another molecular level. However, we are not sure if it is the LUMO + 1 of PCBM or the LUMO of the P3HT. The energy difference between both molecular levels is not big enough (see figure 3.11) to determine it using the data provided by the curves in figure 3.10. Moreover, excited states have lower energy separation among them so that some molecular levels can get partially mixed. In addition, maybe some interface energy levels are being formed in the heterojunction due to the IDIS phenomenon explained in section 1.2 of this thesis. The access to this levels could be the cause of the arising of a "hot - electron" current at -2.1 eV in the P3HT/PCBM heterojunction. It is noticeable that this increase is not visible in the hot - electron device with PCBM. This could mean that the extra level is related to the P3HT, but it could also come from a different way in which the higher levels of PCBM are displaced in energy due to the presence of the P3HT.
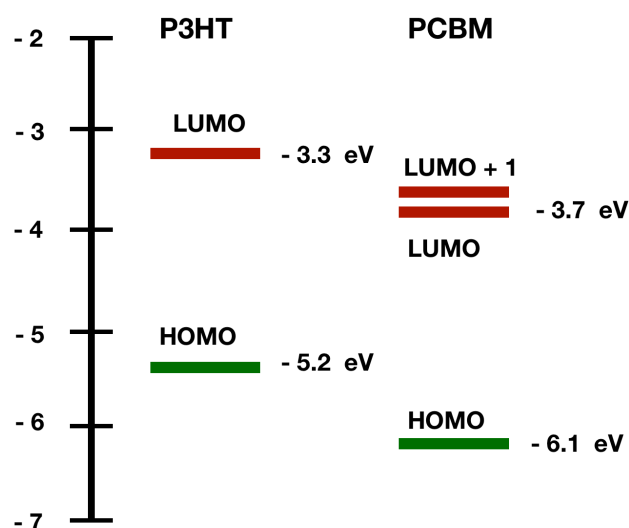

FIGURE 3.11. **Scheme of the molecular levels of P3HT and PCBM in eV.** The LUMO and LUMO +1 molecular levels of PCBM lie energetically close to each other and to the LUMO level of P3HT.

At this point, it seems also important to recall that the results obtained with in device molecular spectroscopy are energy levels of the molecular orbitals relative to the Fermi level of the base metal (in our case gold). This represents an advantage in the sense that, as the measurements are performed in device operative conditions any interface dipole or any interaction at the metal/organic semiconductor interface are implicitly taken into account in our results. Nevertheless, we do not obtain absolute values of the molecular energy levels of the organic materials when they are alone, but relative values

of those energy levels when they are in contact with the base and the collector in device operative conditions.

We also studied the electron injection performance of the devices under different temperatures. The results obtained are shown in figure 3.12. The high noise in the measurements was not surprising. At low temperature, the currents are especially small, of the order of pA, and the signal to noise ratio is consequently reduced. Nevertheless, it is possible to throw some conclusions.

The collector current decreases with temperature. On the one hand, "hot - electrons" have also a thermal energy. If this thermal energy is decreased the overall energy of the "hot - electron" decreases and the current at the tunnel junction drops (see figure 3.3). On the other hand, the diode also has a decreasing current with decreasing temperature, as it consists of a semiconductor. These two phenomena cause a drop in the "hot" current measured at small temperatures (see figure 3.12). This is a positive result, because if the current would increase with a falling temperature, we would have to suspect that what we have is a typical metal behaviour. This could imply the existence of metal filaments through the semiconductor that would connect base and collector, which would invalidate our results. The recipe used for the spin coating and the careful deposition of the top contact on top of the organic layer have prevented this from happening. Fitting the curves obtained at different temperatures, we can verify also that the onset of the "hot" current is independent on the temperature as it should be. The barrier established between Au and OSC is fixed and it is not changing with temperature. This is a further confirmation about the reliability of our measurements and it is also showing us one more time, that the P3HT does not play a role in the injection of electrons, as the behaviours of the two samples are very similar.
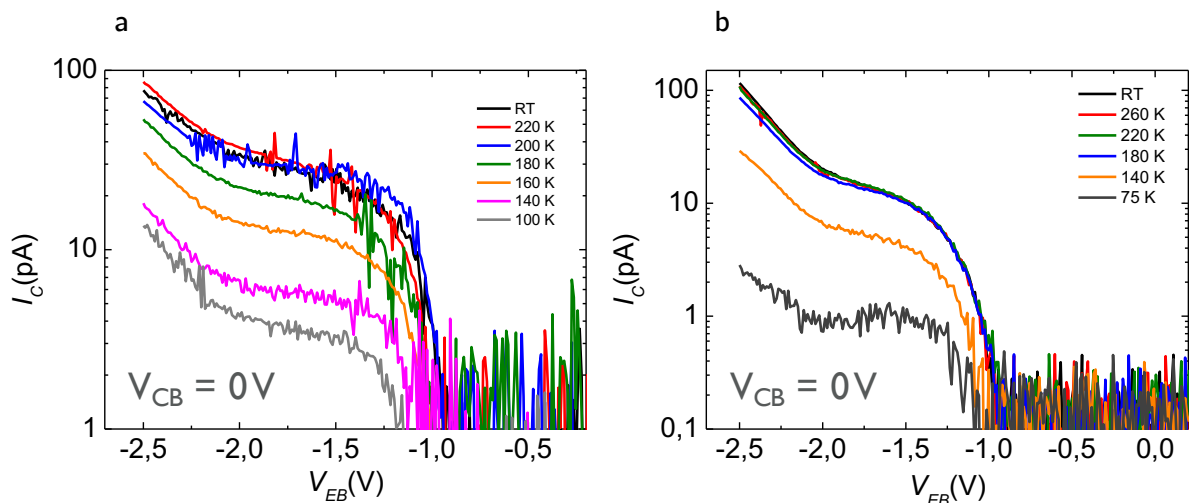

FIGURE 3.12. Hot electron currents at different temperatures in logarithmic scale. a, "Hot - electron" current from an i - *MOS* device with PCBM (a) and P3HT:PCBM (b) at different temperatures in logarithmic scale. No V_{CB} voltage has been applied. The current starts to decrease strongly from 180K to lower temperatures.

4. Conclusions and future perspective

In this thesis we have focused on the study and further development of hot - electron devices for in device molecular spectroscopy of energy barriers in metal/organic semiconductor interfaces. This technique has been performed with solution processed molecules, such as PCBM and a P3HT:PCBM bulk heterojunction. Both organic materials have been studied with three main objectives: the determination of molecular levels in device operative conditions, the study of energy barriers in metal/organic interfaces and the study of the photovoltaic properties and behaviour of the P3HT:PCBM heterojunction in comparison with PCBM.

First, we have explored the energy alignment of Au/PCBM and Au/P3HT:PCBM interfaces. We were able to characterize the LUMO level of PCBM using a vertical device and without any prior material parameter. In addition, we were able to observe another higher energy level in the P3HT:PCBM heterojunction. However, more experiments will be necessary to determine unambiguously if this energy level corresponds to the LUMO + 1 molecular level of PCBM, the LUMO level of P3HT or to interface energy levels formed in the heterojunction due to the IDIS phenomenon.

Second, using the onset of the hot - electron device, we were able to determine the energy barrier of the Au/PCBM and Au/PCBM-P3HT interfaces. In the light of the results it seems that the energy barrier in both cases is the same. In the PCBM and in the P3HT:PCBM devices the current starts to increase at -1.0 eV. This means that the energy difference between the Fermi energy of the gold base and the first available molecular level is 1 eV and it seems that in both situations we are basically measuring the PCBM LUMO level.

Finally, performing two terminal measurements we were able to study the photovoltaic efficiency of the P3HT:PCBM bulk heterojunction in comparison with PCBM. The mixture of a p-type material like P3HT and a photovoltaic n-type material like PCBM seems to increase the efficiency of the photovoltaic cell. This makes sense as p-type materials have an inclination to hole transport and n-type to electron transport. The heterojunction takes advantage of these characteristics of the materials that form it, so that the efficiency increases in comparison with an only n-type material. In our case the efficiency of the bulk heterojunction was 200% the efficiency of PCBM.

The work of this thesis pretends to be a step in the understanding of metal/organic interface energy barriers with the use of in device molecular spectroscopy. However, there are still a lot of steps to make to reach a thorough understanding of this area.

Till now hot - electron devices had been studied with n - type molecules. Now with this thesis, a study has been done with a p-type/n-type heterojunction. It would be interesting to expand the study of p-type/n-type heterojunctions and gather information on the full energy level alignment that could be connected to the photovoltaic effect. For example it seems interesting to determine the reason for the second peak in the i - *MOS* hot electron current curve. More studies need to be carried out to elucidate if this peak is due to the LUMO + 1 of the PCBM, the LUMO of P3HT or other interface phenomena.

Beyond our study, the next logical step could be to try i - *MOS* with ambipolar molecular semiconductors.

5. References

[1] Boehme, C., & Lupton, J. M. (2013). Challenges for organic spintronics. *nature nanotechnology*, *8*(9), 612.

[2] Forrest, S. R. (2004). The path to ubiquitous and low-cost organic electronic appliances on plastic. *Nature*, *428*(6986), 911.

[3] Benfenati, V., Toffanin, S., Bonetti, S., Turatti, G., Pistone, A., Chiappalone, M., ... & Saguatti, D. (2013). A transparent organic transistor structure for bidirectional stimulation and recording of primary neurons. *Nature materials*, *12*(7), 672.

[4] Forrest, S. R. (2004). The path to ubiquitous and low-cost organic electronic appliances on plastic. *Nature*, *428*(6986), 911.

[5] Muccini, M. (2006). A bright future for organic field-effect transistors. *Nature materials*, *5*(8), 605.

[6] Lee, J., Chen, H. F., Batagoda, T., Coburn, C., Djurovich, P. I., Thompson, M. E., & Forrest, S. R. (2016). Deep blue phosphorescent organic light-emitting diodes with very high brightness and efficiency. *Nature materials*, *15*(1), 92.

[7] Holliday, S., Ashraf, R. S., Wadsworth, A., Baran, D., Yousaf, S. A., Nielsen, C. B., ... & Alamoudi, M. (2016). High-efficiency and air-stable P3HT-based polymer solar cells with a new non-fullerene acceptor. *Nature communications*, *7*, 11585.

[8] Bernier, P., Bidan, G., & Lefrant, S. (1999). Advances in synthetic metals: twenty years of progress in science and technology. Elsevier.

[9] Friend, R. H., *et al.* (1999). Electroluminescence in conjugated polymers. *nature*, *397*(6715), 121.

[10] Chamberlain, G. A. (1983). Organic solar cells: A review. *Solar cells*, *8*(1), 47-83.

[11] Burroughes, J. H., Bradley, D. D., Brown, A. R., Marks, R. N., Mackay, K., Friend, R. H., ... & Holmes, A. B. (1990). Light-emitting diodes based on conjugated polymers. *nature*, *347*(6293), 539.

[12] Koezuka, H., Tsumura, A., & Ando, T. (1987). Field-effect transistor with polythiophene thin film. *Synthetic Metals*, *18*(1-3), 699-704.

[13] Sirringhaus, H. (2005). Device physics of solution-processed organic field-effect transistors. *Advanced Materials*, *17*(20), 2411-2425.

[14] Hwang, J., Wan, A., & Kahn, A. (2009). Energetics of metal–organic interfaces: New experiments and assessment of the field. *Materials Science and Engineering: R: Reports*, *64*(1-2), 1-31.

[15] Vázquez, H., Dappe, Y. J., Ortega, J., & Flores, F. (2007). Energy level alignment at metal/ organic semiconductor interfaces:"Pillow" effect, induced density of interface states, and charge neutrality level. *The Journal of chemical physics*, *126*(14), 144703.

[16] Ishii, H., Sugiyama, K., Ito, E., & Seki, K. (1999). Energy level alignment and interfacial electronic structures at organic/metal and organic/organic interfaces. *Advanced materials*, *11*(8), 605-625.

[17] Braun, S., Salaneck, W. R., & Fahlman, M. (2009). Energy-level alignment at organic/metal and organic/organic interfaces. *Advanced materials*, *21*(14-15), 1450-1472.

[18] Ziegler, D., Gava, P., Güttinger, J., Molitor, F., Wirtz, L., Lazzeri, M., ... & Stampfer, C. (2011). Variations in the work function of doped single-and few-layer graphene assessed by Kelvin probe force microscopy and density functional theory. *Physical Review B*, *83*(23), 235434.

[19] Palermo, V., Palma, M., & Samorì, P. (2006). Electronic characterization of organic thin films by Kelvin probe force microscopy. *Advanced materials*, *18*(2), 145-164.

[20] Nonnenmacher, M., o'Boyle, M. P., & Wickramasinghe, H. K. (1991). Kelvin probe force microscopy. *Applied physics letters*, *58*(25), 2921-2923.

[21] Kaiser, W. J., & Bell, L. D. (1990). Direct investigation of subsurface interface electronic structure by ballistic-electron-emission microscopy. In *Electronic Structure of Metal-Semiconductor Contacts* (pp. 252-255). Springer, Dordrecht.

[22] Atxabal, A., Braun, S., Arnold, T., Sun, X., Parui, S., Liu, X., ... & Ortmann, F. (2017). Energy Level Alignment at Metal/Solution-Processed Organic Semiconductor Interfaces. *Advanced Materials*, *29*(19), 1606901.

[23] Gobbi, M., Pietrobon, L., Atxabal, A., Bedoya-Pinto, A., Sun, X., Golmar, F., ... & Hueso, L. E. (2014). Determination of energy level alignment at metal/molecule interfaces by in-device electrical spectroscopy. *Nature communications*, *5*, 4161.

[24] Parui, S. (2013). Hot electron transport in metallic spin valve and graphene-silicon devices at the nanoscale. University of Groningen Library.

[25] Crowell, C. R., & Sze, S. M. (1965). Ballistic mean free path measurements of hot electrons in Au films. *Physical Review Letters*, *15*(16), 659.

[26] N. Balkan (Ed.). (1998). Hot electrons in semiconductors: physics and devices (Vol. 5). Oxford University Press on Demand.

[27] Kajen, R. S., Chandrasekhar, N., Feng, X., Müllen, K., & Su, H. (2011). Vibrational excitations in molecular layers probed by ballistic electron microscopy. *Nanotechnology*, *22*(43), 435701.

[28] Atxabal, A., McMillan, S., Garcia Arruabarrena, B., Parui, S., Llopis, R., Casanova, F., ... & Hueso, L. E. (2019). Strain effects on the energy level alignment at metal/organic semiconductor interfaces. *ACS applied materials & interfaces*.

[29] Arnold, T., Atxabal, A., Parui, S., Hueso, L. E., & Ortmann, F. (2018). Hot Electrons and Hot Spins at Metal–Organic Interfaces. *Advanced Functional Materials*, *28*(15), 1706105.

[30] Nelson, J. (2011). Polymer: fullerene bulk heterojunction solar cells. *Materials today*, *14*(10), 462-470.

[31] Gobbi, M. (2013). *Spintronic devices based on fullerene C60* (Doctoral dissertation, PhD thesis, NanoGune).

[32] Pathak, D., Wagner, T., Adhikari, T., & Nunzi, J. M. (2015). AgInSe2. PCBM. P3HT inorganic organic blends for hybrid bulk heterojunction photovoltaics. *Synthetic Metals*, *200*, 102-108.

[33] LeClair, P. R. (2002). Fundamental aspects of spin polarized tunneling. *Eindhoven University of Technology*.

[34] Tremolet de Villers, B., Tassone, C. J., Tolbert, S. H., & Schwartz, B. J. (2009). Improving the reproducibility of P3HT: PCBM solar cells by controlling the PCBM/cathode interface. *The Journal of Physical Chemistry C*, *113*(44), 18978-18982.

6. Acknowledgements

I would like to finish this thesis thanking the people that have been with me these four years and those who have mentored me this last year during the realization of this thesis.

First of all, I would like to thank Prof. José María Pitarke for giving me the opportunity to do the final degree thesis in NanoGUNE.

I also want to thank my supervisor Prof. Luis Hueso for offering me the opportunity of working in his research group during my summer internship and for his support during the realization of this thesis. You have taught much more things that the ones I can show in this thesis. I have learned from you a lot about research and about the scientific world.

Many thanks to all the members of the nanodevices group for creating such a nice environment and making me feel welcome. To Francesco Calavalle for all your support in the lab and for the delicious coffee breaks. Also to Roger Llopis "el técnico", because without your technical support and your patience my work in the lab woudn't have been possible. Thanks to Kaushik Bairagi for being my express teacher from time to time and for being always so addressable. Thank you also to Elisabetta Zuccatti and Ainhoa Atxabal for helping me in my first steps in nanoGUNE inside and outside the lab and for your encouraging support.

I would like to thank as well my university supervisor Prof. Josu Ortega Aperribay for being always available when I needed help, and for his efficiency and his collaborative spirit.

Finally, thank to all the people that have been always there during the degree. Thanks to my parents, for believing in my even more than I do. Thanks to the rest of my family and friends for lifting me up whenever I needed it. And also thanks to my true colleagues at university, for sharing laughs and tears. Without you my time in university would have been much tougher.

I will always remember with affection all these people that have made these four years a positive and beautiful experience.

Thank you all!